Environ Sci Pollut Res (2014) 21:3503–3514
DOI 10.1007/s11356-013-2329-y

RESEARCH ARTICLE

H_2S photocatalytic oxidation over WO_3/TiO_2 Hombikat UV100

Angela Alonso-Tellez · Didier Robert · Valérie Keller · Nicolas Keller

Received: 17 August 2013 / Accepted: 4 November 2013 / Published online: 20 November 2013

Abstract Hydrogen sulfide (H_2S) is a toxic, corrosive and malodorous compound with damaging effects even when present at a low concentration in air. Consequently, the development of efficient and environmentally friendly remediation technologies as an alternative to conventional techniques is justified for environmental reasons and public concern over human health and well-being. In the context of indoor air quality control, the use of photocatalysis over semiconductor oxides could be a valuable alternative purification technology due to its wide-ranging effect and its easy way of implementation. The superiority of the TiO_2 Hombikat UV100 photocatalyst in comparison with the Aeroxide© TiO_2 P25 standard was already apparent in the UV-A photocatalytic oxidation of H_2S. We report here on the first use of WO_3/TiO_2 UV100 photocatalysts for this reaction. Associating WO_3 to TiO_2 UV100 was not beneficial in terms of semiconductor coupling and of charge transfer between both phases. Even if such coupled wide band-gap oxide semi-conductor photocatalysts suffered from on-flow deactivation due to the formation of poisoning sulfates as ultimate reaction products continuously stored at the surface, by contrast, their ability to strongly lower and delay the release of SO_2 to the gas phase was very positive for maintaining a weak selectivity into the unwanted SO_2 by-product.

Responsible editor: Philippe Garrigues

A. Alonso-Tellez · V. Keller · N. Keller (✉)
Institut de Chimie et Procédés pour l'Energie, l'Environnement et la Santé (ICPEES), CNRS, University of Strasbourg, 25 rue Becquerel, 67087 Strasbourg, France
e-mail: nkeller@unistra.fr

D. Robert
Saint-Avold Antenna, ICPEES, CNRS, Lorraine University and University of Strasbourg, rue Victor Demange, Saint-Avold, France

Keywords TiO_2 · WO_3 · Hydrogen sulfide · Photocatalysis · Sulfates · Semiconductor coupling · XPS surface analysis

Introduction

Hydrogen sulfide (H_2S) is a toxic, corrosive and low-odour-threshold malodorous compound (Mills 1995). Developing efficient and environmentally friendly remediation techniques for treating air polluted with low H_2S concentration as an alternative to technologies like wet scrubbing, biofiltration, thermal incineration, catalysis or adsorption is thus appropriate for environmental reasons and public concern over human health and well-being. In particular, in the context of indoor air quality control, photocatalysis could be a valuable alternative technology due to its wide-ranging effect and its easy way of implementation.

Photocatalysis is an efficient process for removing H_2S from air, even if works devoted to the photocatalytic degradation of H_2S remain scarce by contrast to those on the mineralisation of hazardous organic molecules (Canela et al. 1998; Kataoka et al. 2005; Kato et al. 2005; Kako et al. 2005; Sopyan 2007; Portela 2008a; Portela et al. 2010; Portela et al. 2008; Rasmussen et al. 2010; Alonso-Tellez et al. 2012a, 2012b). It leads to the formation of sulfates as ultimate reaction products accumulate at the catalyst surface and consequently cause on-flow deactivation. The reaction mechanism itself remains to be fully elucidated (Alonso-Tellez et al. 2012a), though it involves SO_2 as oxidation intermediate (Portela 2008a; Portela et al. 2010), and the direct formation of sulfates from H_2S (Canela et al. 1998; Kataoka et al. 2005; Portela 2008a; Portela et al. 2010, 2008). It has also been proposed that SO_2 could be produced by reaction between H_2S and the $SO_4^{\circ-}$ radical formed by the prior oxidation of surface sulfate with a photogenerated hole (Portela et al. 2008; Alonso-Tellez et al. 2012a).

Anatase TiO_2 is still the most efficient semiconductor when used under UV-A light. The value of using TiO_2 Hombikat UV100 (Sachtleben) produced via the sulfate technology with a higher surface area and a smaller crystallite size, in place of TiO_2 P25 standard (Evonik) obtained via the chloride technology, continues to be a matter of debate (Beenakers and Ray 1997; Lindner et al. 1997a, 1997b; Chen and Ray 1998; Alfano et al. 2000; Colon et al. 2001; Vorontsov et al. 2001; Wang et al. 2002; Hidalgo et al. 2002; Ibrahime and de Lasa 2002; Kirchnerova et al. 2005; Doll and Frimmel 2005; Alonso-Tellez et al. 2012b). Even if most of the works deal with liquid phase, contradictory results have been reported dependent on whether the reactions are carried out in gas or liquid phase, and parameters like the TiO_2 content of the reactional slurry seem to play a role (Wang et al. 2002). The larger surface area of UV100 compared with P25 was also put forward as an explanation for the higher resistance to deactivation shown by UV100 when the final reaction product needs to be stored at the catalyst surface.

In particular, in the photocatalytic oxidation of H_2S, the value of using TiO_2 UV100 in place of the TiO_2 P25 standard has been recently reported (Alonso-Tellez et al. 2012b). Despite the lower crystallinity of TiO_2 UV 100, its superior performance was attributed to a higher value of light transmission across the photocatalytic coating consequently allowing more illuminated TiO_2 to operate, and to its higher surface area. This latter permits an increase in H_2S adsorption capacity, proposed to take place on $O–Ti^{4+}$ surface sites through the sulfur atom and in the capacity to generate more OH° radicals. It also results in the possibility of storing larger amounts of poisoning sulfates and of lowering and delaying the SO_2 release to the gas phase, with the maintenance of a weaker selectivity to the unwanted SO_2 by-product. This explained the strong improvement in the photocatalyst deactivation resistance. The smaller crystallite size of UV100 could also lead to a better balance between surface and bulk recombinations.

The efficiency of TiO_2 photocatalysts remains limited by their recombination and adsorption–desorption properties, and semi-conductor coupling with heterojunction formation is a promising way to design TiO_2-based photocatalysts with improved activity (Kamat and Patrick 1992; Serpone et al. 1995a, b; Robert 2007). The value of adding the WO_3 semiconductor to TiO_2 has been put forward for degrading heteroatom-free volatile organic compound pollutants under UV-A irradiation (Do et al. 1994; Martin et al. 1997; Kwon et al. 2000; Keller et al. 2007; Xiao et al. 2009)—for which no catalyst deactivation by surface poisoning is usually observed. It is reported to result from a suitable photogenerated charge separation that limits the recombination rate and from modified adsorption properties. Di Paola et al. have also reported that $WO_3–WS_2$ coupling enhanced the phenol photodegradation, due to electron and hole transfers between WS_2 and WO_3 (Di Paola et al. 2000).

We aim thus at reporting on the first use of WO_3/TiO_2UV100 Hombikat photocatalysts in the UV-A photocatalytic oxidation of H_2S.

Experimental

Catalyst preparation

TiO_2 Hombikat UV100 was supplied by Sachtleben (Germany). WO_3/TiO_2UV100 photocatalytic materials were prepared by impregnating TiO_2UV100 with an excess of aqueous solution of $(NH_4)_{10}W_{12}O_{41}.5H_2O$ (Prolabo, >99.8 %) ammonium paratungstate pentahydrate at pH=4.2, using 5 mL(g of TiO_2)$^{-1}$. After evaporation under strong stirring at room temperature, the materials were dried at room temperature for 2 h and further overnight at 110 °C, before being calcined at 400 °C for 1 h in air (5 °C/min rate). The WO_3 loadings ranged from 5 wt.% to 20 wt.% relative to bare TiO_2.

Characterisation techniques

X-ray diffraction (XRD) measurements were carried out on a D8 Advance Bruker diffractometer ($K\alpha_1$(Cu) radiation at 1.5406 Å in a θ/2θ mode).

Surface area and porosimetry measurements were carried out on a ASAP2010 Micromeritics using N_2 as adsorbant at −196 °C and with a prior outgassing at 200 °C for 1 h for desorbing impurities or moisture. The BET surface area was calculated from the N_2 adsorption isotherms; the micropore surface area was derived using the *t*-plot.

Thermal gravimetry analysis (TGA) and temperature programmed oxidation/mass spectrometry (TPO-MS) were performed using a TGA5000 analyser and an OmniStar (Pfeiffer) spectrometer-coupled AutochemII chemisoption analyser (Micromeritics), respectively, with 20 °C/min heating rate, 80/20 O_2/N_2 mixture and 35 mL/min flow rate.

X-ray photoelectron spectroscopy (XPS) surface characterisation was performed on a ThermoVG Scientific apparatus with a Al $K_\alpha$source (1486.6 eV, 20 eV pass energy). The spectra were decomposed assuming several contributions with Doniach-Sunjic shape and Shirley background subtraction. Sulfur-to-titanium (S/Ti) and tungsten-to-titanium (W/Ti) surface atomic ratios were calculated using the sensitivity factors determined by Scofield. The energy shift due to electrostatic charging was subtracted using the contamination carbon C1s band at 284.6 eV as reference.

Earlier works on TiO_2 P25 have showed that light penetration and reactant diffusion across the coating resulted in the

existence of a reactivity gradient depending on the TiO_2 particle location in the coating, i.e. deep internal or external layers (Portela et al. 2008; Alonso-Tellez et al. 2012a; 2012b). This gradient leads to a gradient in terms of S/Ti surface atomic ratio and of relative contents of surface oxygenated phases along the coating thickness. However, we have no access to such data, since the recovering of the used catalyst from the reactor wall leads to averaging of the characterisation data of used TiO_2, with a stronger influence in the case of high TiO_2 surface density tests. Thus, values derived from XPS spectra corresponded to averaged S/Ti surface atomic ratios and averaged relative contents of surface oxygenated phases.

Experimental device and procedure

The photocatalytic tests were carried out in a 265 mm length single-pass annular Pyrex reactor made of two coaxial tubes (i.d. 22 mm and e.d. 28 mm), through which the reactant mixture was passed. Details of the test apparatus are reported elsewhere (Barraud et al. 2005). Depending on the test conditions, 50 or 420 mg of photocatalyst, corresponding to a surface density of 0.21 or 1.77 mg/cm^2, was evenly coated on the internal side of the 30 mm diameter external tube by evaporating a catalyst-containing aqueous suspension to dryness. The catalyst coated reactor was dried at 110 °C for 1 h in air.

The photocatalytic oxidation of H_2S was carried out with an inlet feed composition as follows: H_2S (15 ppm, i.e. 0.023 mg of H_2S per m^3), air (92 vol.%) and balanced He in dry conditions, with a total flow of 200 mL/min (at 1.77 mg/cm^2 surface density) or 500 mL/min (at 0.21 mg/cm^2 surface density), corresponding to a flow rate of 1.4 or 3.5 cm/s and a residence time of 19 or 7.6 s, respectively. H_2S and SO_2 were analysed online every 3 min by a Pulsed Flame Photometric Detector coupled to a CP-Sil 5 CB column on a Varian 3800 gas-chromatograph.

The photocatalyst was first exposed to the polluted air stream with no illumination until dark-adsorption equilibrium was reached. Then, illumination provided by a 8 W blacklight tube (Philips TL8W/08-BLB-F8T5), with a spectral peak centered at 365 nm and located inside the inner tube of the reactor, was switched on. The irradiance received by the TiO_2 coating was 3.3 mW/cm^2.

The efficiency of the remediation process was expressed in terms of H_2S conversion (C_{H2S}), of SO_2 selectivity (S_{SO2})—expected as low as possible since SO_2 remained an unwanted hazardous gaseous by-product—and of sulfur removal in the gas phase, according to Eqs. 1, 2 and 3.

$$C_{H_2S}(\%) = \frac{[H_2S]_{in} - [H_2S]_{out}}{[H_2S]_{in}} \times 100 \quad (1)$$

$$S_{SO_2}(\%) = \frac{[SO_2]_{out}}{[H_2S]_{in} - [H_2S]_{out}} \times 100 \quad (2)$$

$$\text{Sulfur removal}(\%) = \left(1 - \frac{[H_2S]_{out} + [SO_2]_{out}}{[H_2S]_{in}}\right) \times 100 \quad (3)$$

Depending on the conditions, the duration at total sulfur removal, the deactivation rate expressed in percent per hour and the SO_2 release rate expressed in percent per hour could be also reported. The deactivation rate in Fig. 6 and the SO_2 release rate in Fig. 4, both expressed in percent per hour, correspond to the slope of the linear regression of the conversion decrease over time and to that of the SO_2 selectivity increase over time, respectively.

Results and discussion

Material characterisation

The XRD pattern (not shown, see Colon et al. 2001; Hidalgo et al. 2002) showed that TiO_2 UV100 was composed of anatase as the sole crystallised TiO_2 phase. It had a high specific surface area of 330±15 m^2/g. The large surface area of UV100 resulted from a small primary anatase particle size of 8 nm, and its porosity was attributed to the high agglomeration of such small subparticles into round-shaped particles, generating a high density of small pores, as reported by Colon et al. (2001) and Hidalgo et al. (2002). TiO_2 UV100 has been reported to be partly crystalline and to contain a non-negligible part of amorphous phase beside the crystalline anatase (Jensen et al. 2004). Additional physico-chemical characterisation can be found in other reported works (Colon et al. 2001; Hidalgo et al. 2002; Kirchnerova et al. 2005).

Associating WO_3 to UV100 resulted in a decrease in the surface area of the photocatalyst from 330±15 to 200±20 m^2/g, whatever the tungsten amount. No diffraction peaks assigned to WO_3 could be observed by XRD, except the appearance of a low intensity diffraction peak at $2\theta = 22.8°$ corresponding to the formation of some large 35 nm diameter WO_3 particles for contents greater than 10 %—and thus visible by XRD (not shown). This indicated the high dispersion of tungsten species at the TiO_2 surface and the partial loss of specific surface area. Electron dispersive spectroscopy analysis performed during both scanning and transmission (TEM) electron microscopies as well as elemental analysis confirming the presence of tungsten in the WO_3/TiO_2 samples whatever its loading, although no location of tungsten species could be directly determined by TEM, due to the weak electronic contrast between both oxides and to the high dispersion of tungsten species at the TiO_2 surface.

Figure 1a shows the TGA weight loss recorded on fresh TiO_2 UV100: firstly at low temperature the desorption of molecularly adsorbed water, and subsequently at higher temperature till 500 °C, the TiO_2 surface dehydroxylation, corresponding to a total weight loss of 12 %. By comparison, surface dehydroxylation is observed till 300 °C for the medium surface area TiO_2 P25 (53 m^2/g), with a smaller weight loss of 2 %. The higher dehydroxylation temperature on UV100 could result from the smaller size of the crystallites, whereas the weight loss recorded for both samples was directly proportional to their specific surface areas, i.e. a specific surface ratio of 330/53 for a weight loss ratio of 12/2.

WO_3/TiO_2 UV100 samples had similar TGA profiles to bare UV100, with a weight loss attributed to water release until about 500 °C but with a lower dehydroxylating rate, e.g. 5–6 % for WO_3 contents of 10–20 wt.%. According to the working pH of 4.2, lower than the UV100 isoelectrical point measured at 5.4, tungsten was present in the impregnation solution as $(W_{12}O_{41})^{-10}$ anions (Di Gregorio and Keller 2004) and the TiO_2 surface considered as $TiOH_2^+$, so that the tungsten grafting occurred by means of anionic exchange of $(W_{12}O_{41})^{-10}$ onto –OH surface groups of TiO_2 rather than onto Ti^{4+} sites. This could explain the significant decrease in the hydroxylation rate of the material.

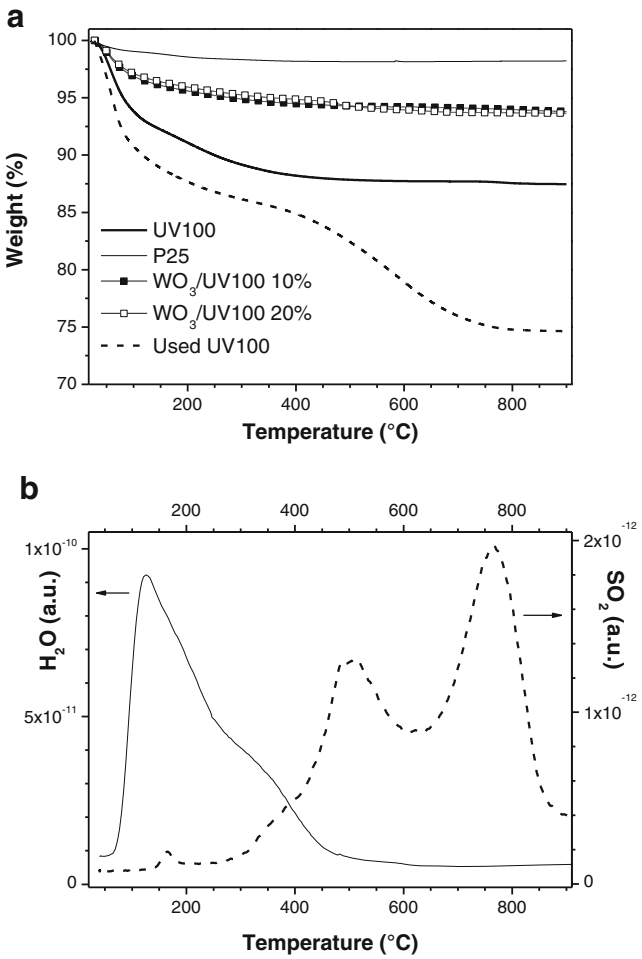

Fig. 1 **a** TGA performed on TiO_2 UV100 and WO_3/UV100 samples (with 10 % and 20 % as examples) as well as on TiO_2 UV100 after test. TGA of fresh TiO_2 P25 is given for comparison. **b** TPO-MS performed on used TiO_2 UV100. Test conditions: $d(TiO_2)$=1.77 mg/cm^2, total flow of 200 mL/min

The Ti *2p* and the O *1 s* region of the XPS spectra recorded on fresh TiO_2 UV100 is shown in Fig. 2. The Ti *2p* spectra evidenced the doublet related to the Ti $2p^{3/2}$–Ti $2p^{1/2}$ spin-orbit components of surface Ti^{4+}, at 458.2 and 463.9 eV, respectively, with no contribution attributed to Ti^{3+} species, indicating the presence of few surface defects (Kubo and Nakahira 2008). A weak high energy asymmetry was however observed that could result from the presence of the non-negligible content of amorphous TiO_2 in the sample, for which a stronger charge effect could be observed during the XPS analysis when compared with crystallised anatase. However, it was not possible to fully rule out the possible presence of some crystallites with characteristic size being largely smaller than the 8 nm mean particle size calculated for UV100 (e.g. 2–3 nm) and for which quantum size effect with higher energy Ti^{4+} centers could thus be observed and which would lead to asymmetric peaks.

Three contributions were observed on the O *1 s* spectra, attributed to O–Ti^{4+}bonds in TiO_2 network, Ti–O–H bonds corresponding to –OH surface groups and oxygen from residual water molecules adsorbed at the surface, accounting for 61 %, 31 % and 8 % relative surface contents, respectively.

Figure 3 shows the W *4f* and the O *1 s* region of the XPS spectra recorded on fresh WO_3/TiO_2 UV100 photocatalytic materials as a function of the WO_3 content, whereas relative contents of oxygenated surface species, as well as W/Ti and $W^{5+}/W^{5+}+W^{6+}$ surface atomic ratios are summarised in Table 1. Whatever the tungsten amount, no difference was observed on the Ti *2p* spectra when compared with that of WO_3 free-UV100, with the doublet related to the Ti $2p^{3/2}$–Ti $2p^{1/2}$ spin-orbit components of Ti^{4+}, at 458.2 and 463.9 eV, respectively (not shown). No additional Ti–O–W bonds were evidenced, in agreement with works of Grandcolas, who noticed the formation of Ti–O–W bonds—with the appearance of a higher energy doublet at about 459.8/465.5 eV—only when the tungsten salt was impregnated onto an amorphous material, before final calcination, and not when impregnation was carried out on an already crystallised support (Grandcolas 2009).

Taking in account the Ti *3p* contribution at 36.9±0.1 eV, whatever the WO_3 content, the W *4f* spectra displayed the presence of both W^{6+} and W^{5+} species, with the 2.3 eV spin-orbit coupling doublets at 35.4–37.7±0.1 and 34.2–36.5±0.1 eV, respectively (Salje et al. 1979; Valigi et al. 2002; Di Gregorio and Keller 2004). Beside the main W^{6+} contribution characteristic of WO_3 oxide, W^{5+} was attributed to partially reduced species in strong interaction with the surface. The

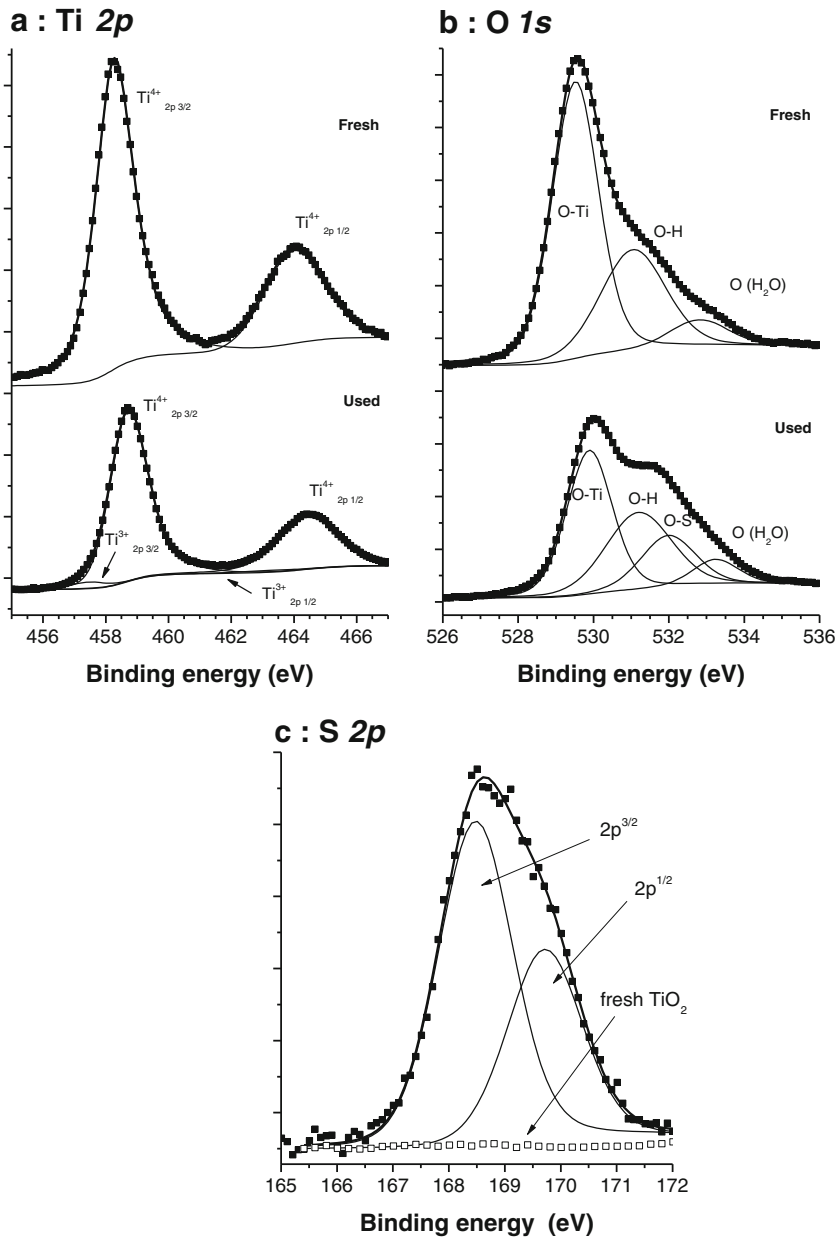

Fig. 2 XPS spectra of **a** Ti*2p*, (**b**) O*1s* and **c** S*2p*, of UV100, fresh and after test. Test conditions: $d(TiO_2)$=1.77 mg/cm^2, total flow of 200 mL/min

W^{5+} relative content, i.e. $W^{5+}/W^{5+}+W^{6+}$ surface atomic ratio, was almost non-dependent on the WO_3 content, whereas the W/Ti surface atomic ratio quasi-linearly increased with the increase in the WO_3 content. This indicates that the increase in the WO_3 content did not result in a loss of dispersion, with no influence on the particle size and the maintenance of a homogenous tungsten deposition at the TiO_2 surface, consistent with the absence of any diffraction peaks and of any oxide nanoparticles that could be assigned to WO_3 on XRD patterns and TEM images, respectively. Indeed, it is known that: (1) at high WO_3 loadings, larger particle sizes would favor in situ partial reduction of WO_3 under the XPS beam and thus would result in an increase in the W^{5+} relative content while (2) at low loadings, larger size WO_3 particles would exhibit weaker interaction with the TiO_2 surface, resulting in a decrease in the W^{5+}content. On WO_3/ZrO_2 systems, Keller and Di Gregorio have observed a shift in the W/Zr linearity already for tungsten contents greater than 10 %, but the commercial ZrO_2 support used displayed a lower surface area of 51 m^2/g versus 330 m^2/g for the UV100 support (Di Gregorio and Keller 2004).

In addition, O *1 s* spectra of WO_3/TiO_2 UV100 displayed an additional contribution arising at 530.7±0.1 eV energy, assigned to O–W bonds (Grandcolas 2009), together with the decrease in the relative content of –OH surface groups from 31 % on bare UV100 down to 8–9 % on WO_3-loaded TiO_2 samples. This was consistent with the hypothesis of anionic surface exchange onto the $TiOH_2^+$ surface, leading to the grafting through the –OH surface groups of TiO_2.

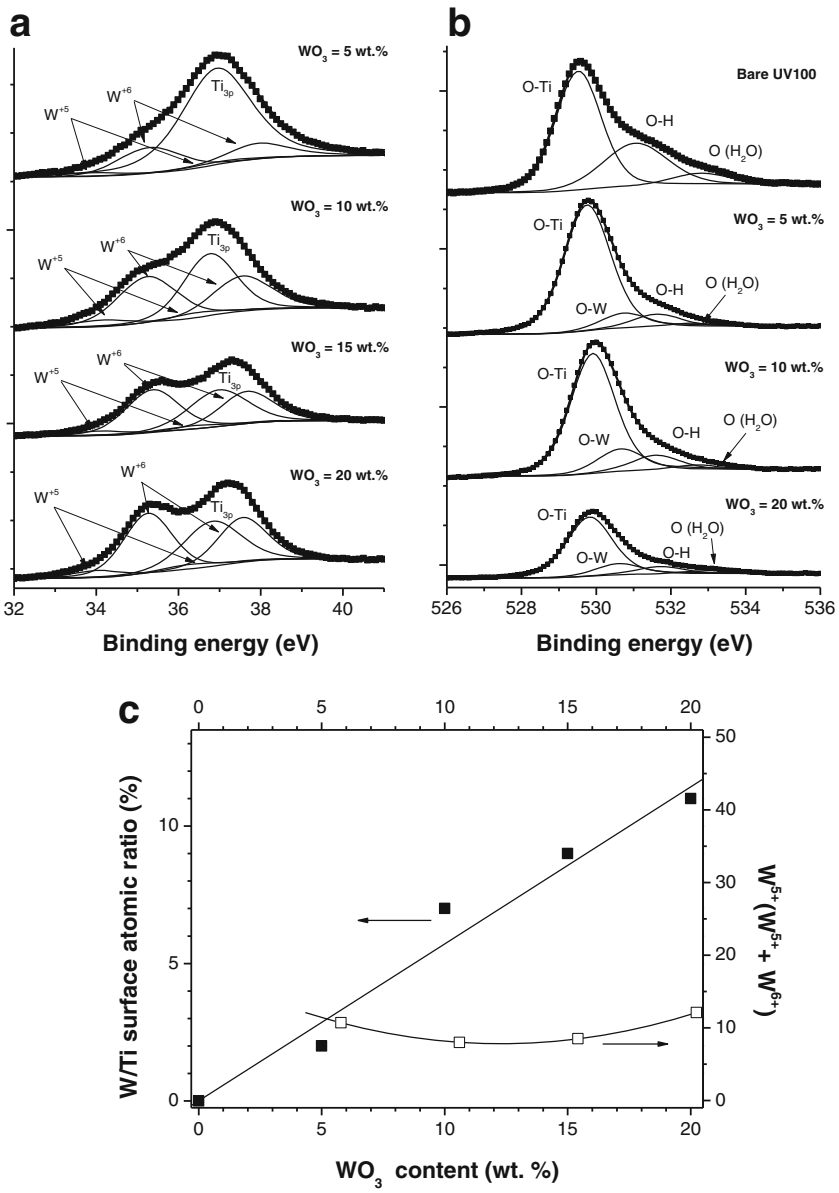

Fig. 3 Influence of the tungsten loading on **a** the W*4f* and **b** the O*1s* XPS spectra of WO_3/TiO_2 UV100, as well as on **c** both W/Ti surface atomic ratio and relative surface content of W^{5+}

Table 1 Averaged relative contents of O–Ti, O–H, O–W, H_2O, O–S surface species, averaged S/Ti, W/Ti and $W^{5+}/W^{5+}+W^{6+}$ surface atomic ratios

Photocatalytic systems		O–Ti %	O–H %	O–W %	O–S %	H_2O%	$W^{5+}/(W^{5+}+W^{6+})$	W/Ti	S/Ti
Fresh	UV100	61	31	–	–	8	–	–	–
	WO_3(5 wt.%)/UV100	80	8	9	–	2	0.12	0.02	–
	WO_3(10 wt.%)/UV100	73	9	14	–	3	0.085	0.07	–
	WO_3(15 wt.%)/UV100	73	9	14	–	3	0.085	0.07	–
	WO_3(20 wt.%)/UV100	73	9	14	–	4	0.11	0.11	–
After test	UV100	42	32	–	18	7	–	–	0.23
	WO_3(5 wt.%)/UV100	44	12	18	20	7	0.18	0.03	0.19
	WO_3(10 wt.%)/UV100	44	13	13	23	8	0.045	0.06	0.24
	WO_3(15 wt.%)/UV100	44	13	13	23	8	0.045	0.06	0.24
	WO_3(20 wt.%)/UV100	41	11	15	25	8	0.18	0.09	0.19

Test conditions: $d(TiO_2)$=1.77 mg/cm^2 , total flow of 200 mL/min

Photocatalytic oxidation of H_2S over WO_3/TiO_2 UV100 materials

In mild reaction conditions

Figure 4 shows the influence of the WO_3 weight content of the WO_3/TiO_2 UV100 systems on the on-stream evolution of the SO_2 selectivity and on the SO_2 release rate (in percent per hour), obtained at complete H_2S conversion for a 1.77 mg/cm^2 surface density and a 200 mL/min total flow. Whatever the WO_3 content, conversions of 100 % were obtained, so that the material efficiency was expressed by the duration at total sulfur removal, before SO_2 was detected in the gas phase, as well as by the SO_2 release rate. Bare UV100 allowed total sulfur removal to be maintained for 37 h before SO_2 was released into the outlet flow, whereas this duration could be extended to 51 h for a WO_3 content of 10 %, which seemed to be the optimal content in respect to this evaluation criterion. Other WO_3/TiO_2 UV100 systems displayed shorter durations at total sulfur removal and even shorter than that obtained on bare UV100 in the case of 5 % and 15 % loadings. However, it was worth observing a decrease of the SO_2 release rate when increasing the WO_3 content, from 3.9 %/h on bare UV100 to 1.5 %/h on WO_3(20 %)/TiO_2 UV100, so that, e.g. the WO_3(20 %)/TiO_2 UV100 sample led to a similar duration of total sulfur removal than bare UV100, but could take advantage of a strongly less-marked SO_2 release rate. The evolution of the SO_2 release rate could be related to the SO_2 surface phenomena with preferential adsorption on WO_3 as discussed later, while the evolution of the duration at total sulfur removal with a maximum for 10 wt.% of WO_3 could result from both SO_2 surface phenomena and changes in the activity of TiO_2-based photocatalysts.

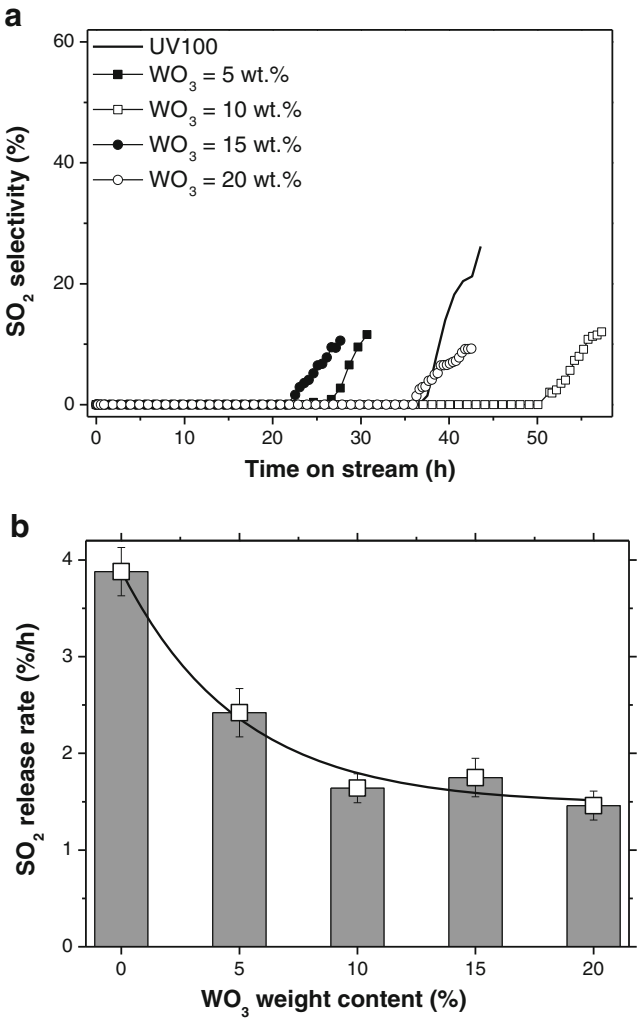

Fig. 4 Influence of the WO_3 weight content of the WO_3/TiO_2 UV100 system on **a** the on-stream evolution of the SO_2 selectivity obtained at complete H_2S conversion and **b** the SO_2 release rate in %/h. The error *bars* result from the uncertainty on the calculation of the linear regression applied on the SO_2 selectivity increase over time. Test conditions: $d(TiO_2)$=1.77 mg/cm^2, total flow of 200 mL/min

TGA/TPO-MS characterisation of the TiO_2 UV100 after test is reported in Fig. 1. TGA curves showed that TiO_2 UV100 displayed after test a larger weight loss when compared with that of the fresh material, i.e. 25 % versus 12 %, together with the release of H_2O and SO_2 molecules. The release of H_2O molecules corresponded first at temperatures lower than 100–150 °C to the desorption of water adsorbed on TiO_2, and subsequently to the dehydration of the surface sulfate species within the 200–400 °C range. At higher temperatures, the weight loss corresponded to the decomposition of surface sulfates, with SO_2 release and no formation of water, the decomposition temperature being reported to be dependent on the photocatalyst nature and on the sulfate/titania interaction (Sohn et al. 2002; Grandcolas 2009; Alonso-Téllez et al. 2012b). After test, the photocatalyst can be considered as a strongly hydrated $Ti(SO_4)/TiO_2$ material, in agreement with the water release till 400 °C and the water contribution in the XPS O *1 s* spectra (see later, in Fig. 2b and reported in Table 1), similarly to $Ti(SO_4)/ZrO_2$ materials (Sohn et al. 2002).

After test, XPS characterisation of TiO_2 UV100 photocatalyst shown in Fig. 2 evidenced a slight shift of 0.5 eV to higher binding energies for Ti^{4+}, as already reported with sulfated titania photocatalysts (Barraud et al. 2005) and in a parametric study of the H_2S photocatalytic oxidation over the TiO_2 P25 reference (Alonso-Tellez et al. 2012a). This upward shift resulted from the increase in effective positive charge around Ti^{4+} surface species, suggesting the direct coordination of titanium atoms to strongly electron-withdrawing SO_4 centers and the existence of an electron transfer from TiO_2 to sulfate anions. A weak intensity doublet contribution was observed at lower energy levels, attributed to the presence of a small amount of Ti^{3+} that could result from the reduction under the H_2S flow of a fraction of Ti^{4+} surface species, as already observed during the DES degradation over low cristallinityTiO_2-based systems (Grandcolas 2009). The S

2p spectra recorded on used TiO_2 showed a broad signal consisting in the S $2p^{3/2}$ –S $2p^{1/2}$ spin-orbit coupling doublet at 168.4 and 169.8 eV, assigned to surface S^{6+}sulfates (Moulder et al. 1992). It was also previously proposed that the S *2p* spectra could be slightly enlarged by: (1) the presence of polysulfates formed by a partial and local polymerisation of sulfates, or by (2) the coexistence at the surface of sulfates with different mono- and bi-chelated coordination modes to Ti^{4+} that would result in a change in the electronic environment of sulfur atoms (Alonso-Tellez et al. 2012a; 2012b; Han et al. 2008).

Whatever the tungsten content of used WO_3/TiO_2 UV100 photocatalysts, no modification was observed on both Ti *2p* (not shown) and S *2p* spectra (e.g. for 10 % of WO_3 in Fig. 5a), when compared with that of bare or WO_3-loaded TiO_2 materials after test. This meant that no additional Ti–O–S bond was formed during the test, since no higher energy doublet was observed on the Ti *2p* spectra (Grandcolas 2009). Also, no additional W–S bonds were formed, since no lower energy doublet around 163 eV was observed on the S *2p* spectra (Martinez et al. 2004). This was confirmed by looking to the W *4f* spectra, on which the signature of W–S bonds should arise as a low energy doublet at about 32.8–35 eV (Salvati et al. 1981; Martinez et al. 2004). In Fig. 5 and in Table 1, similarly to what was observed for fresh WO_3/TiO_2 UV100, both W^{6+} and W^{5+} species were present at the catalyst surface, except for WO_3 contents greater than 10 %, for which an additional low intensity doublet contribution arose at 37.7/40.0±0.1 eV energy, and was attributed to W–O–S bonds, corresponding to sulfur-containing species in interaction with WO_3. This contribution increased with increase in the WO_3 weight content and could correspond preferentially to the signature of surface sulfates connected to WO_3 or to SO_2 molecules in strong interaction with WO_3. However, SO_2 molecules adsorbed on WO_3 were most likely desorbed under ultra-high vacuum. One should note that, in the bonding

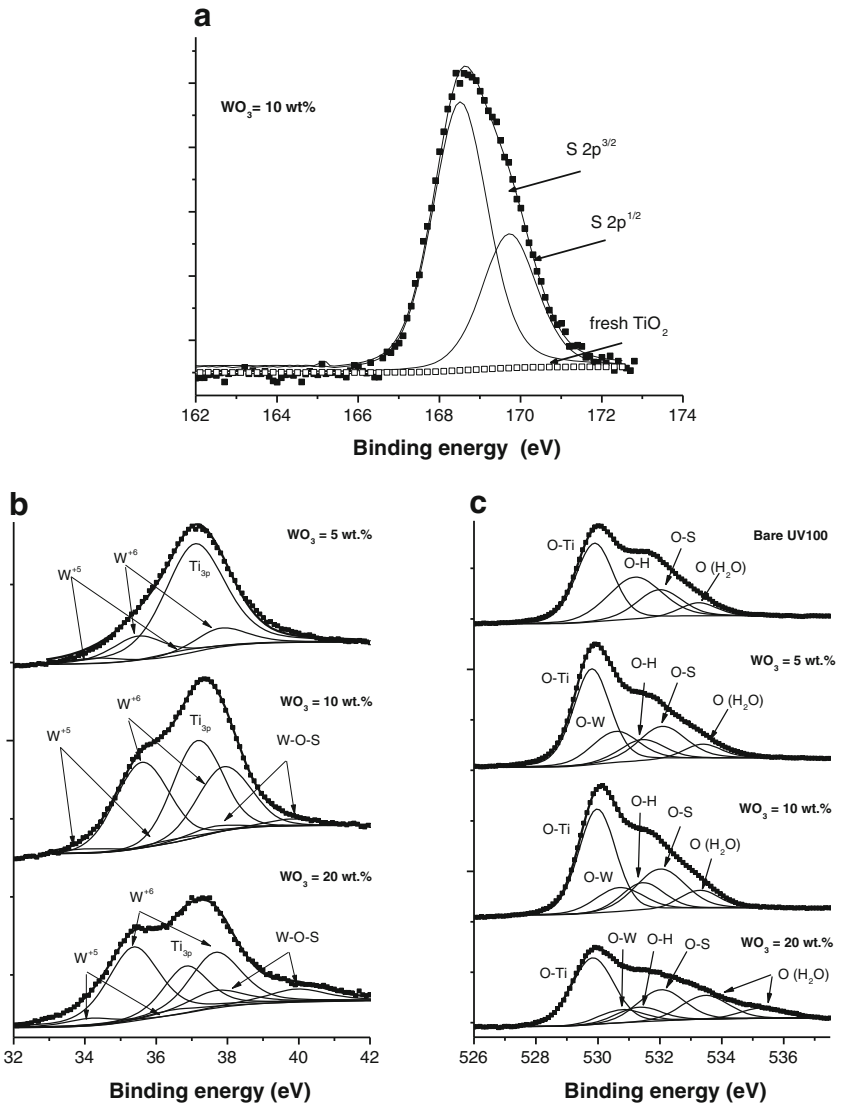

Fig. 5 **a** S *2p* XPS spectra of WO_3(10 %)/UV100, fresh and after test. Influence of the tungsten loading on **b** the W*4f* and **c** the O*1s* XPS spectra of WO_3/TiO_2 UV100 systems after test. Test conditions: d(TiO_2)= 1.77 mg/cm^2, total flow of 200 mL/min

between the sulfates and WO_3 occurring through an oxygen atom, no change in the binding energy of the sulfur atom could be observed on the S *2p* spectra.

In addition to the contributions observed on fresh TiO_2 UV100 and WO_3/TiO_2 UV100 photocatalysts, the O *1 s* spectra shown in Figs. 2 and 5 displayed after the test an additional contribution at 532.1±0.1 eV assigned to O–S bonds (Jung and Grange 2001; Grandcolas 2009; Alonso-Tellez et al. 2012a, 2012b) and corresponded to oxygen bonded to the central atom of sulfur within sulfate species. On bare and on WO_3-loaded TiO_2 UV100 photocatalysts, the averaged $O–Ti^{4+}$ relative content decreased from 61–80 % for the fresh photocatalysts down to 42–44 % after the test. This was accompanied by the maintenance of the averaged O–H relative content and by the increase in the averaged O–S relative content up to 18–25 %. Whatever the photocatalyst, a similar 0.5 eV upward shift was recorded for the $O–Ti^{4+}$ bond from the TiO_2 network, i.e. from 529.6 to 530.1 eV, and was attributed to the presence of the electron-withdrawing SO_4 on the Ti^{4+} center with possible electron transfer from Ti^{4+} to sulfate anions, so that oxygen to Ti^{4+} electron donation could consequently occur within the O–Ti bond. So, similarly to what was proposed in previous works on bare TiO_2 (Alonso-Tellez et al. 2012a, 2012b), we could hypothesise that $O–Ti^{4+}$ surface sites could act as adsorption/reaction sites for H_2S with a first molecular adsorption step on Ti^{4+} through the sulfur atom of H_2S and as storage sites for poisonous sulfates.

However, one could deduce from Table 1 that the averaged W/Ti surface atomic ratio was not affected by the deposition of sulfates at the photocatalyst surface, with the maintenance of the ratio after test at about 0.02, 0.06 and 0.11 for WO_3 contents of 5 %, 10–15 % and 20 %, respectively. So, it could be proposed that no preferential location of sulfates occurred at the surface of WO_3/TiO_2 materials, both titanium and tungsten surface sites being poisoned by sulfates.

In strong reaction conditions

The influence of the WO_3 content on the evolution of both H_2S conversion and SO_2 selectivity, as well as on the calculated deactivation rate and on the performances at $t=20$ h of test, was also studied in stronger reaction conditions, so with a lower TiO_2 surface density and a higher total flow, i.e. 0.21 mg/cm^2 and 500 mL/min, respectively (Fig. 6). Bare UV100 maintained a complete H_2S conversion for durations longer than in the case of WO_3/TiO_2 UV100 systems and suffered from a less marked on-flow deactivation: the deactivation rate increased with increasing the WO_3 loading, from 1.3 %/h from UV100 to 3.6–3.8 %/h for 15–20 % of WO_3. Increasing the WO_3 loading of the system resulted in a decrease in the H_2S conversion recorded at $t=20$ h together with the on-flow deactivation, both being more pronounced with increasing the WO_3 amount. Thus, bare UV100 still displayed the higher conversion but suffered from a high SO_2 selectivity of 75 %, so that the sulfur removal remained weak. By contrast, WO_3/TiO_2 UV100 photocatalysts led to a weak

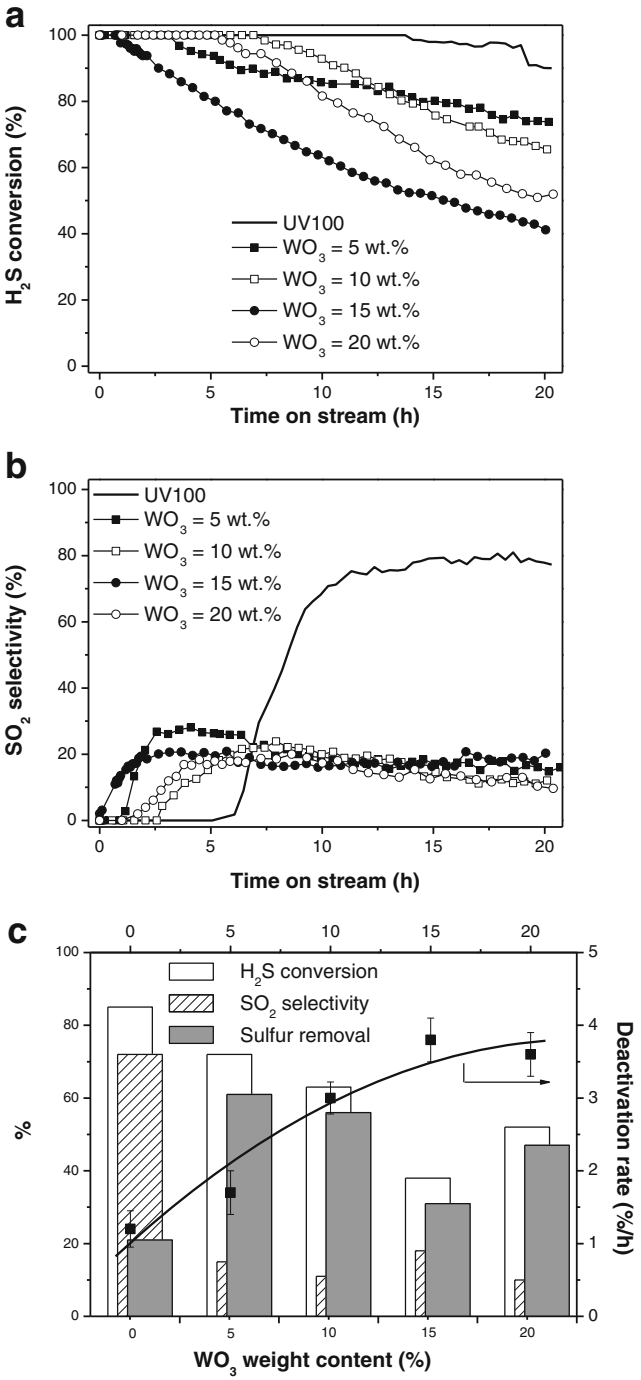

Fig. 6 Influence of the WO_3 weight content of the WO_3/TiO_2 UV100 system on the on-stream evolution of both **a** H_2S conversion and **b** SO_2 selectivity. **c** H_2S conversion, SO_2 selectivity and sulfur removal at $t=$ 20 h of reaction together with the observed deactivation rate. The error *bars* result from the uncertainty on the calculation of the linear regression applied on the conversion decrease over time. Test conditions: $d(TiO_2)=$ 0.21 mg/cm^2, total flow of 500 mL/min

SO_2 selectivity of 15–20 %, whatever the WO_3 content. This allowed the achievement of significantly higher sulfur removal efficiencies when compared with that obtained on bare UV100, with an optimum at 5 wt.% WO_3, for which WO_3/TiO_2 still displayed at t = 20 h a sulfur removal of 61 % versus 21 % for UV100.

So, although WO_3/TiO_2 UV100 deactivated more rapidly with increasing the WO_3 content, this was not related to a higher initial H_2S conversion into surface site-blocking sulfates. Indeed, TGA of used photocatalysts exhibited a less pronounced high temperature weight loss corresponding to the usual signature of sulfates (Fig. 7). By contrast, it displayed an additional low-temperature weight loss within the 200–250 °C range that could be attributed to the desorption of SO_2 stored at the catalyst surface and that could explain the low selectivity into SO_2 recorded. Admittedly, one could claim that such a high initial H_2S conversion could result in the immediate blockage of the surface by sulfates, but this remained very unlikely in regards to the high surface area available and to the lower high-temperature weight losses measured by TGA. So, in contrary to bare TiO_2 UV100, the sulfur-containing reaction products at the surface of WO_3/TiO_2 UV100 systems after test were proposed to be adsorbed SO_2 molecules in addition to sulfates.

Influence of WO_3 in the WO_3/TiO_2 UV100 system

Taking into account the faster on-flow deactivation of WO_3/TiO_2 UV100 systems, it has been proposed that, in the case of the H_2S photocatalytic oxidation, associating WO_3 with TiO_2 UV100 would not necessarily be positive in terms of coupling and that the WO_3/TiO_2 UV100 systems might not take advantage from a charge transfer between both phases. This negative behavior—contrary to the positive coupling between WO_3 and TiO_2 in the case of the P25 standard—could result from the smaller crystallite size of UV100 at about 8 nm that could be adequate to achieve a compromise between surface and volume recombination, in comparison to the larger crystallite size of anatase in P25 at 19 nm. Indeed, Zhang et al. (1998) have already observed an optimal particle size at about 10 nm in the chloroform decomposition on calibrated anatase nanoparticles, resulting from a compromise between bulk and surface recombinations, preponderant for too large and too small particle sizes, respectively (Kortan et al. 1990; Linsebigler et al. 1995; Serpone et al. 1995a, b; Hagfeldt and Grätzel 1995; Hoffmann et al. 1995; Hines and Guyot-Sionnest 1996).

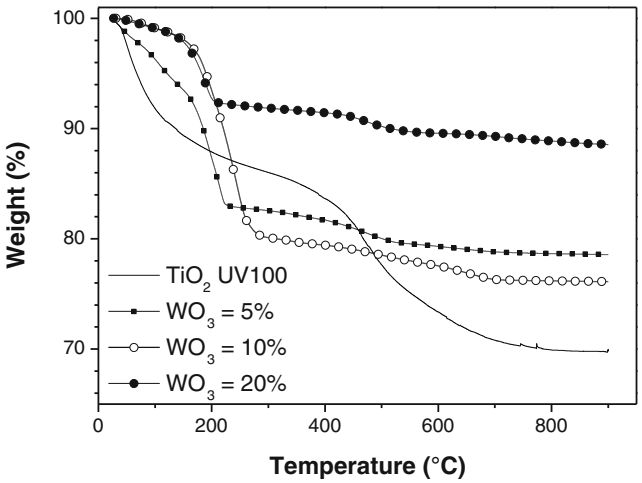

Fig. 7 TGA of used WO_3/TiO_2 UV100 samples. Test conditions: $d(TiO_2)$=0.21 mg/cm^2, total flow of 500 mL/min

In addition, the high dispersion of WO_3 on TiO_2 UV100 could unfortunately be an obstacle to achieving improved performances, in the sense that highly dispersed tungsten-based phases could excessively decrease the number of available active sites at the TiO_2 surface, since O–Ti^{4+} surface sites have been proposed as adsorption sites for H_2S with a first molecular adsorption step on Ti^{4+} through the sulfur atom of H_2S.

Even if the existence of an anatase/rutile coupling within TiO_2 structures is a matter of debate, one could also put forward that the absence of any rutile phase in UV100 would avoid the possible establishment of a WO_3/anatase/rutile three-phase semiconductor coupling that could take place in WO_3/TiO_2 P25 systems due to the presence of both anatase and rutile phases. Indeed, such a three-phase semiconductor coupling was put forward in WO_3/β-SiC–TiO_2 photocatalysts for explaining the high efficiency in the degradation of methylethylketone shown by the ternary photocatalytic material in comparison to that obtained on the different corresponding binary systems (Keller and Garin 2003).

One could propose that the sulfates at the surface of WO_3/TiO_2UV100 are in interaction with both oxide semiconductors. So, (1) sulfates could be preferentially located at the WO_3/TiO_2 interface, as a result of the driving force exerted by the surface acidity provided by the addition of WO_3 particles that would favour the migration of sulfates from TiO_2 to the WO_3/TiO_2 interface. Or, (2) sulfates could separately be formed at the surface of both TiO_2 and WO_3 semi-conductors, either by direct reaction with photogenerated holes of each oxide, or through the reaction with OH° radicals.

However, one could propose that associating WO_3 with UV100 could play a positive role by maintaining a weak and stable SO_2 selectivity, due to the ability of WO_3/TiO_2 UV100 to hinder the SO_2 release to the gas phase due to preferential adsorption phenomena. Indeed, it has been proposed that SO_2 could preferentially adsorb on WO_3 or, e.g. at the WO_3/TiO_2 interface, so that the increase in the WO_3 content can decrease the SO_2 release rate. This would also result in a shorter diffusion path for SO_2 at the photocatalyst surface before reaching the WO_3 semi-conductor, in favour of a lower release to the gas phase. The reaction mechanism of the

photocatalytic oxidation of H_2S and SO_2 under UV-A light remains to be fully elucidated, but, hypothesising that the consecutive oxidation of the SO_2 intermediate into surface sulfate could occur via $O_2^{\circ-}$ superoxide radicals, explains that fewer sulfates were formed at the surface of WO_3/TiO_2 UV100 photocatalysts, since the reduction of O_2 into $O_2^{\circ-}$ by a photogenerated electron cannot proceed at the conduction band of WO_3. Photogenerated electrons at the conduction band of WO_3 could directly be formed by the activation of the WO_3 semi-conductor or result from the interphase transfer from that of activated TiO_2. The lowering and delay in the hazardous SO_2 pollutant release in regards to the sulfate production was also recently pointed out by Rasmussen et al. (2010) for explaining the very low SO_2 selectivity exhibited by TiO_2/MCM-41-based mesoporous systems or hybrid chemisorption/photocatalysis TiO_2–SiM_gO_x composites.

Conclusion

WO_3/TiO_2UV100 Hombikat photocatalysts were first used in the photocatalytic oxidation of H_2S under UV-A light. Similarly to bare TiO_2 photocatalysts, they suffered from on-flow deactivation due the formation of sulfates as ultimate reaction products accumulating at the photocatalyst surface. It has been proposed that associating WO_3 to TiO_2 UV100 was not beneficial in terms of semi-conductor coupling and charge transfer between both wide band-gap oxides. However, the influence of WO_3 on the performances of WO_3/TiO_2 UV100 photocatalysts was strongly dependent on the WO_3 weight content. Among the hypotheses, the small particle size of UV100 at about 8 nm could perhaps already be optimal to achieve a compromise between surface and volume recombination, and the high dispersion of WO_3 on the UV100 material could unfortunately lower the number of Ti^{4+} surface sites, on which initial molecular adsorption of H_2S was proposed to take place through the sulfur atom of H_2S. However, the ability of the WO_3/TiO_2 UV100 photocatalysts to strongly lower and delay the SO_2 release to the gas phase was very positive in terms of maintaining a weak selectivity into the unwanted SO_2 by-product. This was thought to result from preferential adsorption on WO_3 and from the absence of any further oxidation of SO_2 reaction intermediate into surface sulfates by $O_2^{\circ-}$ radicals at the conduction band of WO_3.

Acknowledgments The authors thank the EU for supporting this work, performed in the frame of the 6th FP EFFORTS European project–Effective Operation in Ports–FP6-031486. Sachtleben (Germany) is thanked for providing the TiO_2 product. P. Bernhardt (LMSPC) is gratefully acknowledged for having performed XPS characterisation.

References

Alfano OM, Bahnemann D, Cassano AE, Dillert R, Goslich R (2000) Photocatalysis in water environment using artificial and solar light. Catal Today 58:199–230

Alonso-Tellez A, Robert D, Keller N, Keller V (2012a) A parametric study of the UV-A photocatalytic oxidation of H_2S over TiO_2. Appl Catal B Environ 115–116:209–218

Alonso-Tellez A, Robert D, Keller N, Keller V (2012b) Comparison on Hombikat UV-100 and P25 TiO_2 performance in gas-phase photocatalytic oxidation reactions. J Photochem Photobiol A Chem 250: 58–65

Barraud E, Bosc F, Edwards D, Keller N, Keller V (2005) Gas phase photocatalytic removal of toluene effluents on sulfate titania. J Catal 235(2):318–326

Beenakers AACM, Ray AK (1997) Novel swirl-flow reactor for kinetic studies of semiconductor photocatalysis. AIChE J 43: 2571–2578

Canela MC, Alberici R, Jardim WF (1998) Gas phase destruction of H_2S using TiO_2 UV–vis. J Photochem Photobiol A Chem 112:73–80

Chen D, Ray AK (1998) Photodegradation kinetics of 4-nitrophenol in TiO_2 suspension. Water Res 32(11):3223–3234

Colon G, Hidalgo MC, Navio JA (2001) Photocatalytic deactivation of commercial TiO_2 samples during simultaneous photoreduction of Cr (VI) and photooxidation of salicylic acid. J Photochem Photobiol A Chem 138:79–85

Di Gregorio F, Keller V (2004) Activation and isomerisation of hydrocarbons over WO_3/ZrO_2 catalysts. I. Preparation, characterization and X-ray photoelectron spectroscopy studies. J Catal 225:45–55

Di Paola A, Palmisano L, Augugliaro V (2000) Photocatocalytic behavior of mixed WO_3/WS_2 powders. Catal Today 58:141–149

Do YR, Lee W, Dwight K, Wold A (1994) The effect of WO_3 on the photocatalytic activity of TiO_2. J Solid State Chem 108:198–201

Doll TE, Frimmel FH (2005) Photocatalytic degradation of carbamazepine, clofibric acid and iomeprol with P25 and Hombikat UV100 in the presence of natural organic matter (NOM) and other organic water constituents. Water Res 39:403–411

Grandcolas M (2009) Titanium dioxide based materials and textiles for the photocatalytic degradation of chemical warfare agents. Ph.D. Thesis

Hagfeldt A, Grätzel M (1995) Light-induced redox reactions in nanocrystalline systems. Chem Rev 95:49–68

Han ST, Zhang GY, Xi HL, Xu DN, Fu XZ, Wang XX (2008) Sulfated TiO_2 decontaminate 2-CEES and DMMP in vapor gas. Catal Lett 122:106–110

Hidalgo MC, Colon G, Navio JA (2002) Modification of the physicochemical properties of commercial TiO_2 samples by soft mechanical activation. J Photochem Photobiol A Chem 148:341–348

Hines MA, Guyot-Sionnest P (1996) Synthesis and characterization of strongly luminescing ZnS-capped CdSe nanocrystals. J Phys Chem 100:468–471

Hoffmann MR, Martin ST, Choi W, Bahnemann DW (1995) Environmental applications of semiconductor photocatalysis. Chem Rev 96:69–96

Ibrahime H, de Lasa H (2002) Photocatalytic conversion of air borne pollution effect of catalytic type and catalyst loading in a novel photo-CREC-air unit. Appl Catal B Environ 38:201–213

Jensen H, Joensen KD, Jørgensen J-E, Pedersen JS, Søgaard EG (2004) Characterization of nanosized crystalline photocatalyst. J Nanoparticle Res 6:519–526

Jung SM, Grange P (2001) Evidence of correlation between electronic density and surface acidity of sulfated TiO_2. Catal Lett 76:27–30

Kako T, Irie H, Hashimoto K (2005) Prevention against catalytic poisoning by H_2S utilizing TiO_2 photocatalyst. J Photochem Photobiol A Chem 171:131–135

Kamat PV, Patrick B (1992) Photophysics and photochemistry of quantized zinc oxide colloids. J Phys Chem 96:6829–6834

Kataoka S, Lee E, Tejedor-Tejedor MI, Anderson MA (2005) Photocatalytic degradation of hydrogen sulfide and in situ FT-IR analysis of reaction products on surface of TiO_2. Appl Catal B Environ 61:159–163

Kato S, Hirano Y, Sano T, Takeuchi K, Matsuzawa S (2005) Photocatalytic degradation of gaseous sulfur compounds by silver-deposited titanium dioxide. Appl Catal B Environ 57:109–115

Keller V, Garin F (2003) Photocatalytic behaviour of a new composite ternary system: WO_3/SiC-TiO_2. Effect of the coupling of semiconductors and oxides in photocatalytic oxidation of methylethylketone in the gas phase. Catal Commun 4:377–383

Keller N, Barraud E, Bosc F, Edwards D, Keller V (2007) On the modification of photocatalyst improving visible light and UV degradation of gas-phase toluene over TiO_2. Appl Catal B Environ 70: 423–430

Kirchnerova J, Herrera Cohen M-L, Guy C, Klavan D (2005) Photocatalytic oxidation of n-butanol under fluorescent visible light lamp over commercial TiO_2 (Hombicat UV100 and Degussa P25). Appl Catal A Gen 282:321–332

Kortan AR, Hull R, Opila RL, Bawendi MG, Steigrwald ML, Carroll PJ, Brus LE (1990) Nucleation and growth of CdSe on ZnS quantum crystallite seeds, and vice versa, in inverse micelle media. J Am Chem Soc 112:1327–1332

Kubo T, Nakahira A (2008) Local structure of TiO_2-derived nanotubes prepared by the hydrothermal process. J Phys Chem 112:1658–1662

Kwon YT, Song KY, Lee WI, Choi GJ, Do YR (2000) Photocatalytic behavior of WO_3-loaded TiO_2 in an oxidation reaction. J Catal 191: 192–199

Lindner M, Bahnemann DW, Hrithe B, Griebler WD (1997a) Solar water detoxification: novel TiO_2 powders as highly active photocatalysts. J Sol Energy Eng 119:120–125

Lindner M, Theurich J, Bahnemann DW (1997b) Photocatalytic degradation of organic compounds accelerating the process efficiency. Water Sci Technol 35:79–86

Linsebigler AL, Lu G, Yates JT (1995) Photocatalysis on TiO_2 surfaces: principles, mechanisms and selected results. Chem Rev 95:735–758

Martin C, Solana G, Rives V, Marci G, Palmisano L, Sclafani A (1997) Physico-chemical properties of WO_3/TiO_2systemsemployed for 4-nitrophenol photodegradation in aqueous medium. Catal Lett 49: 235–243

Martinez H, Benayad A, Gonbeau D, Vinatier P, Pecquenard B, Levasseur A (2004) Influence of the cation nature of high sulfur content oxysulfide thin films MOySz (M=W, Ti) studied by XPS. Appl Surf Sci 236:377–386

Mills B (1995) Review of methods of odour control. Filtr Sep 2:147–152

Moulder JF, Stickle WF, Sobol PE, Bombon DE (1992) Handbook of X-ray photoelectron spectroscopy. Cahstain J (ed) Perkin Elmer Corporation, Eden Prairie, Minnesota, US

Portela R (2008a) Photocatalytic removal of H_2S in air with TiO_2 supported on UV-A transparent substrates. Ph.D. Thesis, Santiago de Compostela University, Spain

Portela R, Canela MC, Sánchez B, Marques FC, Stumbo AM, Tessinari RF, Coronado JM, Suárez S (2008) H2S photodegradation by TiO2/M-MCM (M : Cr or Ce): deactivation and by-products generation under UV-A and visible light. Appl Catal B Environ 84(3–4):643–650

Portela R, Suarez S, Rasmussen SB, Arconada N, Castro Y, Duran A, Avila P, Coronado JM, Sanchez B (2010) Photocatalytic-based strategics for H_2S elimination. Catal Today 151:64–70

Rasmussen SB, Portela R, Suarez S, Coronado JM, Rojas-Cervantes M-L, Avila P, Sanchez B (2010) Hybrid $TiO_2-SiMgO_x$ composite for combined chemisorption and photocatalytic elimination of gaseous H_2S. Ind Eng Chem Res 49:6685–6690

Robert D (2007) Photosensitization of TiO_2 by M_xO_y and M_xS_y nanoparticles for heterogeneous photocatalysis applications. Catal Today 122:20–26

Salje E, Carley AF, Roberts MW (1979) The effect of reduction and temperature on the electronic core levels of tungsten and molybdenum in WO_3 and $W_xMo_{1-x}O_3$. A photoelectron spectroscopic study. J Solid State Chem 29:237–251

Salvati L, Makovsky LE, Stencel JM, Brown FR, Hercules DM (1981) Surface spectroscopic study of tungsten-alumina catalyst using X-ray photoelectron, ion scattering and Raman spectroscopies. J Phys Chem 85:3700–3707

Serpone N, Lazless D, Khairutdinov R, Pelizzeti E (1995a) Subnanosecond relaxation dynamics in TiO_2 colloidal sols particle sizes (Rp=1.0–13.4). Relevance to heterogeneous photocatalysis. J Phys Chem 99:16655–16661

Serpone N, Maruthamuthu P, Pichat P, Pelizzetti E, Hidaka H (1995b) Exploiting the interparticle electron transfer process in the photocatalysed oxidation of phenol, 2-chlorophenol and pentachlorophenol: chemical evidence for electron and hole transfer between coupled semiconductors. J Photochem Photobiol A Chem 85:247–255

Sohn JR, Kim JG, Kwon TD, Park EH (2002) Characterization of titanium sulfate supported on zirconia and activity for acid catalysis. Langmuir 18:1666–1673

Sopyan I (2007) Kinetic analysis on photocatalytic degradation of gaseous acetaldehyde, ammonia and hydrogen sulfide on nanosized porous TiO_2 films. Sci Technol Adv Mater 8:33–39

Valigi M, Gazzoli D, Pettiti I, Mattei G, Colonna S, de Rossi S, Ferraris G (2002) WO_x/ZrO_2 catalysts: part 1. Preparation, bulk and surface characterization. Appl Catal A Gen 231:159–172

Vorontsov AV, Savinov EN, Davidov L, Smirniotis PG (2001) Photocatalytic destruction of gaseous diethyl sulfide over TiO_2. Appl Catal B Environ 32:11–24

Wang CY, Rabani J, Bahnemann DW, Dohrmann JK (2002) Photonic efficiency and quantum yield of formaldehyde formation from methanol in the presence of various TiO_2 photocatalysts. J Photochem Photobiol A Chem 148:169–176

Xiao MW, Wang LS, Huang XJ, Wu YD, Dang Z (2009) Synthesis and characterization of WO_3/titanate nanotubes nanocomposites with enhanced photocatalytic properties. J Alloys Compd 470(1–2): 486–491

Zhang Z, Wang CC, Zakaria R, Ying JY (1998) Role of particle size in nanocrystalline TiO_2-based photocatalysts. J Phys Chem B 102(52): 10871–10878